# Non-seagrass carbon contributions to seagrass sediment blue carbon

**Matthew P. J. Oreska** ,[1]* **Grace M. Wilkinson,**[1,2] **Karen J. McGlathery,**[1] **Molly Bost,**[3] **Brent A. McKee**[3]
[1]Department of Environmental Sciences, University of Virginia, Charlottesville, Virginia
[2]Ecology, Evolution, and Organismal Biology, Iowa State University, Ames, Iowa
[3]Department of Marine Sciences, University of North Carolina at Chapel Hill, Chapel Hill, North Carolina

## *Abstract*

Non-seagrass sources account for ~ 50% of the sediment organic carbon (SOC) in many seagrass beds, a fraction that may derive from external organic matter (OM) advected into the meadow and trapped by the seagrass canopy or produced in situ. If allochthonous carbon fluxes are responsible for the non-seagrass SOC in a given seagrass bed, this fraction should decrease with distance from the meadow perimeter. Identifying the spatial origin of SOC is important for closing seagrass carbon budgets and "blue carbon" offset-credit accounting, but studies have yet to quantify and map seagrass SOC stocks by carbon source. We measured sediment $\delta^{13}C$, $\delta^{15}N$, and $\delta^{34}S$ throughout a large (6 $km^2$), restored *Zostera marina* (eelgrass) meadow and applied Bayesian mixing models to quantify total SOC contributions from possible autotroph sources, *Z. marina*, *Spartina alterniflora*, and benthic microalgae (BMA). *Z. marina* accounted for < 40% of total meadow SOC, but we did not find evidence for outwelling from the fringing *S. alterniflora* salt-marsh or OM advection from bare subtidal areas. *S. alterniflora* SOC contributions averaged 10% at sites both inside and outside of the meadow. The BMA fraction accounted for 51% of total meadow SOC and was highest at sites furthest from the bare subtidal-meadow edge, indicative of in situ production. $^{210}Pb$ profiles confirmed that meadow-enhanced sedimentation facilitates the burial of in situ BMA. Deducting this contribution from total SOC would underestimate total organic carbon fixation within the meadow. Seagrass meadows can enhance BMA burial, which likely accounts for most of the non-seagrass SOC stored in many seagrass beds.

Seagrass meadows accumulate organic carbon ($C_{org}$) within their beds from seagrass and from the burial of non-seagrass organic matter (OM; Gacia et al. 2002; Hendriks et al. 2008; Fourqurean et al. 2012). Seagrass bed sediment $C_{org}$ (sediment organic carbon [SOC]) $\delta^{13}C$ ratios are typically depleted relative to associated seagrass tissue, irrespective of seagrass species and location (average depletion = 6.3‰), which suggests that non-seagrass sources contribute ~ 50% of the SOC in many meadows (Kennedy et al. 2010). Multiple studies point to the burial of particulate organic matter (POM) as the likely explanation for this non-seagrass fraction (e.g., Campbell et al. 2015; Huang et al. 2015) and, therefore, identify this SOC as allochthonous relative to the seagrass meadow (Howard et al. 2014; Greiner et al. 2016). Meadow canopies trap suspended particles through filtration and by attenuating currents, which contribute to bed accretion (Hendriks et al. 2008; Duarte et al. 2013). However, studies that investigate seagrass SOC composition seldom consider $C_{org}$ spatial origin. If advected POM contributes significantly to seagrass bed accretion, we should observe SOC isotope composition spatial gradients that change with distance from an external source or boundary.

Identifying the source of SOC remains a challenge in most subtidal habitats. Carbon fixed in one area is often exported to adjacent habitats (Duarte and Cebrián 1996; Cebrián et al. 1997), where it might be buried (Middelburg et al. 1997; Zonneveld et al. 2010), remobilized, or respired (Regnier et al. 2013; Hyndes et al. 2014). According to Duarte and Cebrián (1996), more seagrass and marsh production is exported than buried in situ. Particulate organic carbon (POC), dissolved organic carbon (DOC), and dissolved inorganic carbon (DIC) fluxes often connect different habitats, especially over short distances (Cai 2011; Hyndes et al. 2014), which make tracking the generation, transport, and ultimate fate of autotrophic production difficult (Bouillon and Connolly 2009; Bauer et al. 2013; Hyndes et al. 2014). These linkages complicate efforts to assess net ecosystem metabolism in many coastal habitats (Gattuso et al. 1998; Borges et al. 2006; Cai 2011). Spatial gradients have, nevertheless, been used to successfully identify POC and DOC exchanges between adjacent mangrove and seagrass habitats

*Correspondence: mpo4zx@virginia.edu

Additional Supporting Information may be found in the online version of this article.

(Heminga et al. 1994; Bouillon et al. 2007) and marsh DOC and DIC "outwelling" (e.g., Tzortziou et al. 2011). In a coupled marsh-seagrass system, contributions from marsh POC outwelling should be discernable as a change in SOC isotope composition with distance into the seagrass bed.

Interest in financing seagrass restoration through the sale of blue carbon offset-credits (e.g., Nellemann et al. 2009; Murray et al. 2011; Hejnowicz et al. 2015) adds urgency to these questions about seagrass SOC source. A framework now exists for greenhouse gas benefit accounting in seagrass habitats, the Verified Carbon Standard Methodology VM0033 (Emmer et al. 2015), which allocates offset-credits for net autotrophic production resulting from seagrass restoration activities within a specified project area. Offset-credits are not allocated under the framework for allochthonous $C_{org}$ buried in the meadow, because carbon fixed outside the project area cannot necessarily be attributed to project activities (Commission for Environmental Cooperation [CEC] 2014). Restoration projects must, therefore, quantify the autochthonous and allochthonous SOC fractions, presumably using unique isotope or biomarker signatures to identify different autotroph contributors (e.g., Volkman et al. 2008; Oakes and Eyre 2014). However, these chemical signatures often overlap, and isotope ratio measurement variability sometimes inhibits confident percent source estimation (Fry 2007). Howard et al. (2014) tentatively suggest an allochthonous carbon compensation factor (i.e., deduction) of 50% for seagrass meadows, based on the average non-seagrass SOC contribution of 50% found by Kennedy et al. (2010), but this percentage may not be accurate for carbon crediting purposes. The number might be an overestimate, because some non-seagrass $C_{org}$ in the bed likely derives from in situ autotrophs, including epiphytes (Serrano et al. 2015). Alternatively, 50% may be an underestimate, because the average SOC $\delta^{13}C$ values used to generate this figure include a high number of mid-meadow sample sites, and we would expect allochthonous SOC percent contributions to be even higher near meadow edges.

This study investigates whether stable isotopes in seagrass sediment OM exhibit spatial variation that can be used to identify the geographic origin of non-seagrass SOC. The *Zostera marina* (eelgrass) meadow in South Bay, Virginia, U.S.A., is part of the Virginia Coast Reserve Long-Term Ecological Research (VCR-LTER) eelgrass restoration and represents the single largest, successfully restored seagrass meadow to date (Orth et al. 2006, 2012; Orth and McGlathery 2012). SOC profile comparisons confirm that this meadow now stores significantly more SOC than adjacent bare sites (McGlathery et al. 2012; Greiner et al. 2013) and that much of this SOC is non-seagrass in origin (Greiner et al. 2016). However, the SOC is nonuniformly distributed. Percent OM and SOC concentrations decline with distance from the adjacent barrier island (Oreska et al. 2017)—a spatial distribution that suggests "outwelling" from the island's fringing marsh as a possible carbon source vector. The South Bay meadow is part of a coupled seagrass-marsh system, where marsh scarp erosion potentially supplies sediment to the seagrass bed (McGlathery et al. 2013; Fig. 1). Greiner et al. (2016) quantified carbon sources at a single site within this seagrass bed but lacked an adequate tracer to distinguish between the two vascular plants in this system, the seagrass *Z. marina* and the salt marsh cordgrass *Spartina alterniflora*. The authors did, however, find that more than 50% of the $C_{org}$ at their meadow sample site was apparently algal in origin. If allochthonous *S. alterniflora* and algae contribute significant amounts of carbon to the bed SOC pool, their percent contributions should increase with proximity to particular meadow boundaries. We hypothesized that (1) *S. alterniflora* POM inputs account for the SOC spatial gradient that increases with proximity to the fringing marsh on the east side of the meadow (Wreck Island Marsh in Fig. 1), and that (2) the algal carbon percent contribution increases with proximity to the meadow-bare subtidal boundary (the meadow edge that does not adjoin Wreck Island Marsh in Fig. 1), which would be indicative of canopy filtration of allochthonous, algal POM.

## Methods

### Site description

South Bay occurs on the Atlantic side of the southern Delmarva Peninsula, between Wreck Island and Mockhorn Island, Virginia. The central part of the restored meadow now covers an area approximately 6 $km^2$ in size. The Wreck Island fringing marsh adjoins the *Z. marina* meadow to the east, and the Man and Boy Marsh sits opposite Man and Boy Channel to the northwest (Fig. 1). Tides enter and exit the meadow area via Sand Shoal Inlet to the north and New Inlet to the south. This system is oligotrophic—dissolved organic nitrogen averages $11.8 \pm 1.6$ (SE) $\mu$M and dissolved inorganic phosphorous averages $0.5 \pm 0.1$ (SE) $\mu$M over a year (McGlathery et al. 2001)—and experiences low total dissolved nitrogen loading relative to other shallow estuaries, 1 g N $m^{-2}$ $yr^{-1}$ (Tyler et al. 2001; McGlathery et al. 2007). Phytoplankton are present but not abundant in the outer coastal bays in this system on account of the low nutrient inputs (McGlathery et al. 2001; Tyler et al. 2001; Hondula 2012). Water column chlorophyll *a* peaks around 5 $\mu$g $L^{-1}$ in the outer bays during the summer and declines to $< 1$ $\mu$g $L^{-1}$ during the fall; in comparison, average benthic chlorophyll can exceed 80 mg $m^{-2}$ (McGlathery et al. 2001). Cultured bivalves in this system rely primarily on macroalgae and, to a lesser extent, benthic diatoms, the dominant primary producers in the coastal bays along with *Z. marina* (McGlathery et al. 2001; Hondula and Pace 2014). Likely SOC sources in this system are, therefore, *Z. marina*, the only seagrass species, macro- and benthic microalgae (BMA), and *S. alterniflora*, the dominant species in the surrounding salt marshes

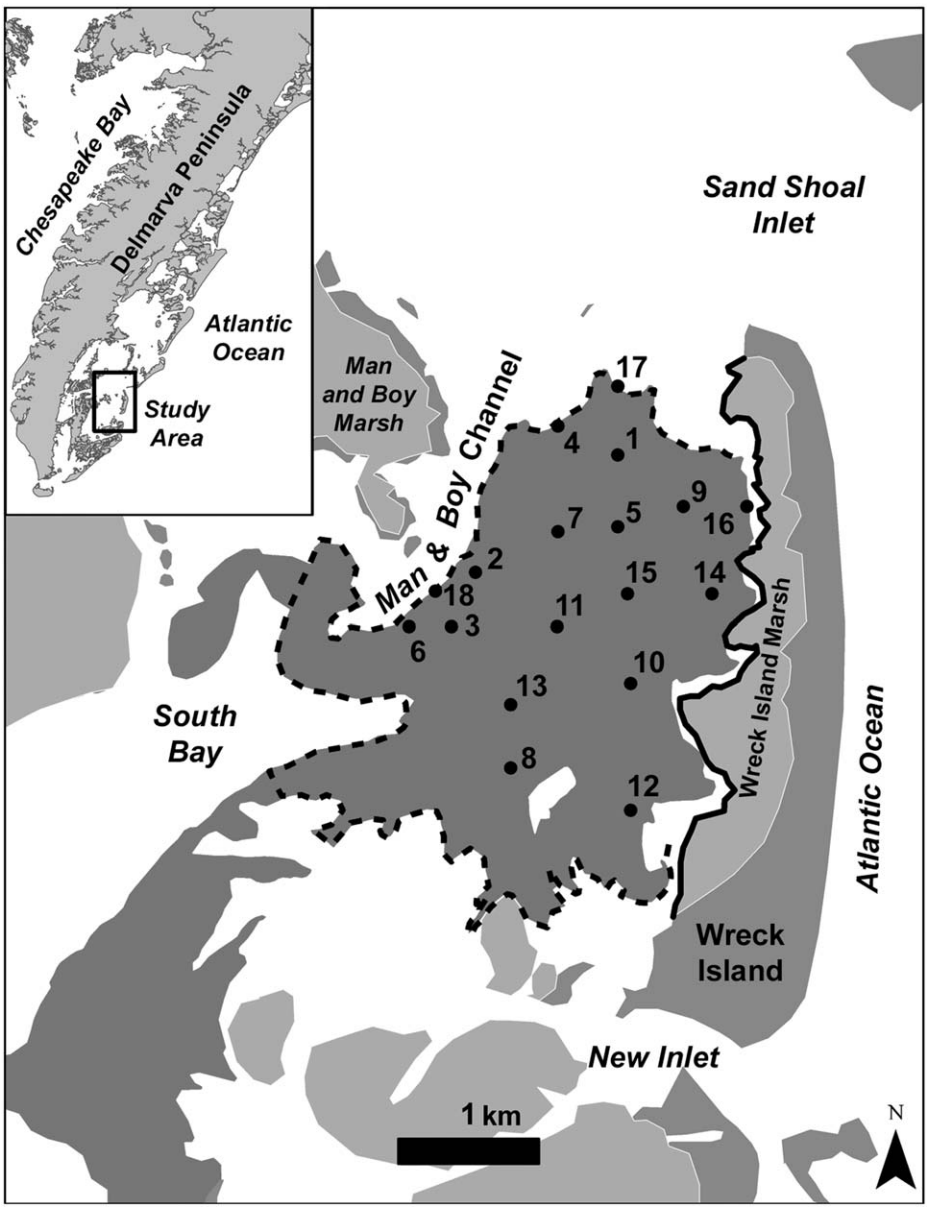


**Fig. 1.** Study Area: The restored *Z. marina* meadow fills the area between Man & Boy Channel and Wreck Island; Two Euclidean distance measures were determined for each meadow site: site distance to Wreck Island Marsh (solid black line) and site distance to the meadow-bare subtidal edge (dashed line); two bare sites were also sampled immediately outside this meadow-bare subtidal boundary (sites 17 and 18).

(Hondula and Pace 2014; Greiner et al. 2016). Dominant macroalgal species include *Ulva lactuca*, *Gracilaria vermiculophylla*, and *Codium fragile*, which are common on tidal flats but generally contribute < 5% of SOC observed at bare and vegetated subtidal sites (McGlathery et al. 2007; Greiner et al. 2016).

**Sample collection**

Three replicate sediment samples were collected using 60 cc hand cores at each of 16 randomly selected sites within the South Bay meadow and at two bare sites immediately adjacent to the meadow during July 2014. The bare sites were located 3 m (site #17) and 13 m from the meadow edge (site #18 in Fig. 1). Past studies have observed OM and SOC concentration peaks between 3 cm and 6 cm below the sediment–water interface in this meadow, the zone of maximum *Z. marina* root and rhizome biomass (Cole and McGlathery 2012; Greiner et al. 2013; Oreska et al. 2017). The sediment samples collected in this study exactly captured this 3–6 cm bed depth interval. A $^{210}$Pb dated core collected from this meadow indicated that the top ~ 5 cm of the bed accumulated following meadow reestablishment; in

contrast, a nearby bare site showed no bed accretion (Greiner et al. 2013). The 3–6 cm interval within the seagrass bed, therefore, receives SOC inputs from multiple pathways: SOC buried due to particulate trapping by the meadow canopy—potentially including allochthonous POM—$C_{org}$ accumulation from decomposing seagrass biomass, and $C_{org}$ from seagrass root exudates. By omitting the top 3 cm on the bed, we excluded the zone of active sediment resuspension and mixing to obtain a relatively stable, time-averaged SOC sample. Compaction was approximately 7% in our cores, on account of their relatively small size and the fact that the sediment in this system is predominantly fine sand (Oreska et al. 2017). Macroscopic root, rhizome, and shell fragments were removed from sediment samples prior to analysis to isolate SOC from belowground biomass (BGB), following methods used previously in this system (Greiner et al. 2013, 2016; Oreska et al. 2017). Refractory roots and rhizomes did not occur in all of our core samples. Homogenizing individual roots or rhizomes would have biased particular sediment samples in favor of *Z. marina*, thereby affecting the meadow-wide sediment isotope distribution results. Sediment samples were dried for 48 h at 60°C and homogenized. We determined the inorganic carbon (IC) fraction by conducting element analysis using a Carlo Erba NA 2500 Element Analyzer on samples ashed in a muffle furnace at 500°C for 6 h, following Fourqurean et al. (2014).

We verified that the 3–6 cm depth interval included SOC burial due to bed accretion by collecting and dating additional sediment cores using the same $^{210}$Pb methods employed by Greiner et al. (2013). Sediment cores were collected in July 2014 at two sites: a meadow site on an original restoration seed plot (site #5 in Fig. 1) and a bare site adjacent to Man and Boy Channel (site #18 in Fig. 1). The meadow site core analyzed in this study was collected from the northwest half of the meadow, which had lower SOC storage (Oreska et al. 2017), for comparison with the Greiner et al. (2013) meadow core, which was collected in an original seed plot in the southeast half of the meadow (located between sites #10 and 15 in Fig. 1). The Greiner et al. (2013) bare site was located northeast of site #17. Profiles were determined to a depth of 20 cm using $^{210}$Pb (22.3 yr half-life), which we compared with the two profiles obtained by Greiner et al. (2013). The cores were divided into 1-cm intervals, which were dated at the University of North Carolina Department of Marine Sciences. $^{210}$Pb activities were determined via isotope-dilution alpha spectrometry for the $^{210}$Pb granddaughter isotope $^{210}$Po, which are in secular equilibrium with each other (Flynn 1968; Matthews et al. 2007). Supported $^{210}$Pb was formed by in situ production of $^{210}$Pb within sediment grains from the decay of $^{222}$Rn. Unsupported $^{210}$Pb was the activity supplied from the atmosphere that adsorbs to particles that then settle into the seagrass sediments, excess $^{210}$Pb that was used to quantify sedimentation rates (Appleby and Oldfield 1983). We noted that excess $^{210}$Pb activities decreased in a non-exponential manner, so a constant rate of supply (CRS) model was applied to profiles within each core, which allows for variable sedimentation over time (Sanchez-Cabeza and Ruiz-Fernández 2012). Carbon accumulation rates were calculated by multiplying the sedimentation rate (cm $yr^{-1}$) for each sediment interval by its bulk $C_{org}$ value.

We considered potential SOC source contributions from three types of autotrophs: *Z. marina*, *S. alterniflora*, and BMA, represented in this system primarily by benthic diatoms (Hondula and Pace 2014). Phytoplankton were not considered as a possible source, both because of their low abundance relative to BMA (McGlathery et al. 2001) and because phytoplankton appear isotopically similar to BMA in this system (Hondula and Pace 2014). *Z. marina* biomass ($n = 4$) and *S. alterniflora* biomass ($n = 4$) grab samples were collected from randomly located sites in the meadow and in Wreck Island Marsh in July 2014 to constrain the stable isotope ranges for these end-members. The *Z. marina* and *S. alterniflora* biomass samples were divided into aboveground biomass (AGB) and BGB fractions, which were dried, ground, and analyzed separately to determine whether these fractions yielded different isotope values. The AGB and BGB values were then averaged to generate individual plant averages, which were subsequently averaged to generate end-member averages. Benthic diatom isotope values for this system were determined by Hondula and Pace (2011, 2014), using a vertical migration sampling approach (cf. Riera and Richard 1996). We limited the mixing model analysis to isotope ratios obtained from the VCR-LTER (Supporting Information). Seston samples were collected on three separate occasions in July 2014 using an 80 $\mu$m tow net to determine whether *S. alterniflora* contributes to POM in this system. We evaluated seston as a possible vector connecting the marsh to the seagrass sediment carbon pool by comparing average seston isotope ratios with end-member isotope ratios, not as a separate end-member with a unique isotopic signature. Plant biomass and seston samples were dried for 48 h at 60°C and homogenized prior to stable isotope analysis.

All sediment, end-member biomass, and seston sample stable isotope compositions were measured at the Marine Biological Laboratory (MBL) Stable Isotope Laboratory in Woods Hole, Massachusetts, U.S.A. Sample carbon, nitrogen, and sulfur percentages and $\delta^{13}$C, $\delta^{15}$N, and $\delta^{34}$S stable isotope ratios were determined using a Europa 20-20 continuous-flow isotope ratio mass spectrometer interfaced with a Europa ANCA-SL elemental analyzer. We considered $\delta^{34}$S as a possible additional tracer, because *Z. marina* and *S. alterniflora* exhibit nonoverlapping $\delta^{34}$S ranges in this system (Harbeson 2010). All isotope ratios were related to their respective international standards and reported using per mil (‰) notation. The analytical precision based on replicate analyses of isotopically homogeneous international standards was ± 0.1‰.

**Bayesian mixing model**

We used Bayesian mixing models to determine whether the observed isotopic spatial variation reflected different autotrophic source contributions to different locations within the meadow. Proportional contributions from the three major autotrophs in this system were calculated for each site. Discrete solutions can be obtained for mixing models, provided the number of sources exceeds the number of tracers used in analyses by $n + 1$. Bayesian mixing models incorporate both observed data and uncertainty to quantify the likelihood of a given solution, which is obtained from the posterior distribution. We conducted three-source (*Z. marina*, *S. alterniflora*, and BMA), two-tracer ($\delta^{13}C$, $\delta^{15}N$) Bayesian mixing model analyses using Stable Isotope Analysis in R (SIAR package version 4.2), which employs isotope ratio means and standard deviations for each end-member (Inger et al. 2010). Previous studies conducted in the VCR-LTER have successfully used Bayesian mixing models to differentiate between these autotrophs in mixed isotope assemblages (Hondula and Pace 2014; Greiner et al. 2016). $\delta^{34}S$ values were ultimately excluded from this analysis, because of observed discrepancies between the $\delta^{34}S$ ranges of the sediment samples and potential end-members. The mixing model analysis did not require a separate IC term, because sediment sample IC was found to be $< 0.1\%$. Diagenetic factors can result in a $1.5‰$ change in $\delta^{13}C$ and a $1.2‰$ change in $\delta^{15}N$ in some systems (Jankowska et al. 2016). We did not include a specific diagenesis term in the model, because past work in this system suggests that diagenetic effects on end-member $\delta^{13}C$ and $\delta^{15}N$ isotope ratios are nominal (Greiner et al. 2016). Even if diagenetic effects are evident at particular sites, sample differences on the order of 1–2‰ should not substantially change mixing model results.

The following equations relate end-member contributions to the sediment at each site:

$$\delta^{13}C_{Sed} = (\phi_Z \times \delta^{13}C_Z) + (\phi_S \times \delta^{13}C_S)$$
$$\delta^{13}N_{Sed} = (\phi_Z \times \delta^{13}N_Z) + (\phi_S \times \delta^{13}N_S)$$
$$1 = \phi_Z + \phi_S + \phi_{BD}$$

Where $\delta^{13}C$ and $\delta^{15}N$ were isotope ratios measured in sediment and in the end-members (Z, S, and BMA).

We ultimately ran the three-source, two-tracer mixing model on both individual sites and on sites binned according to SOC concentration, because certain individual sites exhibited flattened distributions. We grouped meadow sites into four, spatially discrete categories based on their SOC concentrations relative to the meadow SOC mean ($5.85 \pm 1.86$ [SD] mg $C_{org}$ $cm^{-3}$): "lowest" sites with concentrations < the meadow mean − 1 SD, "low" sites with concentrations between the mean − 1 SD and the mean, "high" sites with concentrations between the mean and the mean + 1 SD, and "highest" sites with concentrations > the mean + 1 SD. The bare sites provided a fifth SOC group, with concentrations < 3.1 mg $C_{org}$ $cm^{-3}$. Well-constrained posterior distribution results for these groups allowed us to calculate the bulk SOC contribution from each autotroph source within each meadow SOC zone. We multiplied the fractional contribution results by the average bulk SOC concentration measured in each zone.

**Distribution analyses**

We compared isotope spatial variability relative to the documented SOC spatial gradient within the seagrass bed (Oreska et al. 2017) by mapping average site SOC concentrations and isotope ratios determined from the sediment samples collected during this study. Interpolated SOC, $\delta^{13}C$, $\delta^{15}N$, and $\delta^{34}S$ distributions were generated using kriging. We fit circular, exponential, spherical, stable, and Gaussian semivariogram models to each dataset in ArcGIS 10.2, Geostatistical Analyst. The most robust kriged map for each isotope distribution was selected by cross-validating root mean square errors.

We used the results of the mixing model analysis to address our specific spatial hypotheses: (1) the marsh SOC fraction should decrease with distance from Wreck Island Marsh and (2) the *Z. marina* fraction should increase with distance from the meadow-bare subtidal boundary (the "edge") on account of allochthonous SOC contributions. Site isotope ratios and Bayesian mixing model source fraction posterior means were regressed against site distance from the Wreck Island Marsh and from the meadow-bare subtidal edge using the lm analysis (stats package) in R version 3.2.1. Euclidean distances from the two meadow boundaries were determined for each site using Near analysis in ArcGIS 10.2 (Fig. 1). Data were normally distributed according to the Shapiro-Wilks test (shapiro.text, stats package). The homogeneity of variance assumption was met.

## Results

Core dating using $^{210}Pb$ confirmed that the seagrass bed has accreted due to sediment accumulation, resulting in high, recent SOC accumulation rates. The meadow core obtained from site #5 indicated that the top 5+ cm of the bed at that site have accumulated since the restoration began. In comparison, the bare profile from site #18 had a $^{210}Pb$ profile with low ($\sim 0.6$ dpm $g^{-1}$) activities, typical of nondepositional environments with supported activity only. The $^{210}Pb$ profile for site #5 was similar to that measured by Greiner et al. (2013) (Fig. 2). Activities were higher in the top 11 cm (0.74–1.55 dpm $g^{-1}$), indicating the presence of excess $^{210}Pb$. A CRS model applied to quantify sedimentation rates for the upper 11 cm of this core yielded a similar rate increase to the increase observed in the Greiner et al. (2013) meadow site core, from approximately 0.1 cm $yr^{-1}$ before restoration began in 2000 to 0.6 cm $yr^{-1}$ at the time of core

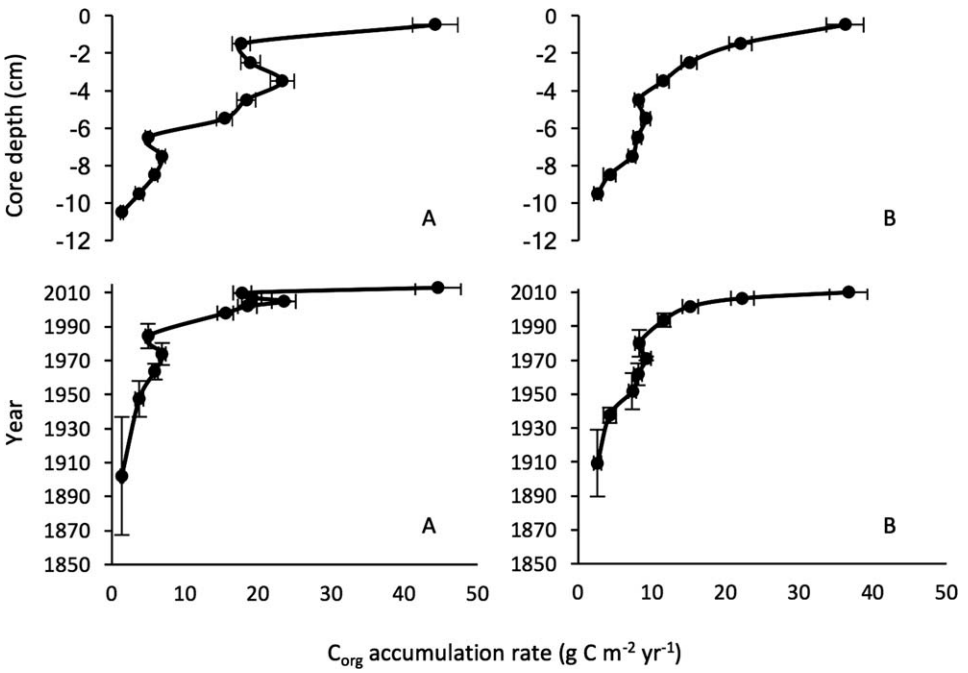


**Fig. 2.** (**A**) Bed depth- and age-calibrated $C_{org}$ accumulation profiles for meadow site 5 and (**B**) for a mid-meadow site analyzed in 2011 by Greiner et al. (2013) (adapted with permission). $^{210}Pb$ dating indicates that the top > 5 cm of the bed at site 5 has accreted since the meadow restoration began in 2000. Bare control sites analyzed in this study (site 18) and by Greiner et al. (2013) were nondepositional.

collection. This sedimentation rate translated to a recent C burial rate > 44 g $C_{org}$ $m^{-2}$ $yr^{-1}$ at site #5 (Fig. 2).

The different autotrophs in this system exhibited different ranges for the different stable isotopes, especially $\delta^{13}C$. The *Z. marina* samples collected during this study yielded $\delta^{13}C$ values from −8.79‰ to −9.92‰; whereas, the *S. alterniflora* values ranged from −13.36‰ to −13.72‰. Regarding $\delta^{15}N$, *Z. marina* values ranged from 6.48‰ to 7.26‰ and *S. alterniflora* values ranged from 7.20‰ to 9.86‰. In comparison, $\delta^{34}S$ provided less of a basis for differentiating *Z. marina* and *S. alterniflora*, due to notable $\delta^{34}S$ enrichment in *Z. marina* AGB and depletion in *Z. marina* BGB. The *Z. marina* AGB $\delta^{34}S$ ranged from 3.89‰ to 10.22‰; whereas, the BGB ranged from −12.52‰ to −5.77‰. *S. alterniflora* showed less $\delta^{34}S$ enrichment, yielding a range for AGB and BGB samples of −8.59‰ to 0.25‰. BMA showed greater average $\delta^{13}C$ depletion and greater average $\delta^{15}N$ and $\delta^{34}S$ enrichment than *Z. marina* or *S. alterniflora* (Table 1). In comparison, seston $\delta^{13}C$ and $\delta^{15}N$ averaged $-14.62 \pm 0.55$ (SE) ‰ and $9.41 \pm 0.31$ (SE) ‰, respectively, a similar isotopic composition to *S. alterniflora*. Seston $\delta^{34}S$ values averaged $5.36 \pm 1.76$ (SE) ‰.

The meadow SOC concentration averaged $5.85 \pm 0.46$ (SE) mg $C_{org}$ $cm^{-3}$ across all 16 meadow sites, but average concentrations at individual sites varied depending on relative location within the meadow. The meadow-wide SOC distribution was kriged using a spherical semivariogram and exhibited anisotropy, with concentrations varying along a predominantly northwest to southeast axis. Kriging the SOC distribution confirmed that the aforementioned SOC site groups were spatially discrete and distributed along a discernable spatial gradient (Fig. 3). SOC concentrations were generally highest near Wreck Island and decreased with proximity to the meadow edge. Four sites in the northwest meadow yielded concentrations < 1 SD below the meadow average, averaging $3.44 \pm 0.21$ (SE) mg $C_{org}$ $cm^{-3}$. Three sites yielded concentrations between the meadow average and −1 SD, averaging $4.96 \pm 0.37$ (SE) mg $C_{org}$ $cm^{-3}$. Five sites yielded "high" concentrations, between the meadow average and +1 SD, averaging $6.42 \pm 0.21$ (SE) mg $C_{org}$ $cm^{-3}$. And four sites in the mid-meadow yielded the "highest" concentrations, > +1 SD above the meadow average and averaging $8.21 \pm 0.15$ (SE) mg $C_{org}$ $cm^{-3}$. The two bare sites adjacent to the meadow yielded an average concentration of $2.82 \pm 0.24$ (SE) mg $C_{org}$ $cm^{-3}$, which was similar to the background SOC concentration measured at a third bare site in nearby Hog Island Bay, $2.93 \pm 0.16$ (SE) mg $C_{org}$ $cm^{-3}$.

The $\delta^{13}C$ and $\delta^{15}N$ data also exhibited spatial gradients. The $\delta^{13}C$ distribution was best fit by an exponential semivariogram, and like the SOC distribution, exhibited anisotropy. Average $\delta^{13}C$ values at sites showed increasing enrichment with distance from Wreck Island, ranging from −17.03‰ up to −12.66‰ (Table 2). The $\delta^{15}N$ distribution was best fit by a circular semivariogram and also showed isotope enrichment with distance from the island, with values ranging from

**Table 1.** End-member stable isotope ratios used in the mixing model analysis.

| | | Mean $\delta^{13}C$ | SD $\delta^{13}C$ | Mean $\delta^{15}N$ | SD $\delta^{15}N$ | Mean $\delta^{34}S$ | SD $\delta^{34}S$ |
|---|---|---|---|---|---|---|---|
| *Zostera* | Whole plant | −9.37 | 0.55 | 6.79 | 0.34 | −0.17 | 2.41 |
| | AGB ($n = 4$) | −8.99 | 0.83 | 7.13 | 0.35 | 7.89 | 2.92 |
| | BGB ($n = 4$) | −9.88 | 0.37 | 6.44 | 0.45 | −8.24 | 2.99 |
| *Spartina* | Whole plant | −13.67 | 0.15 | 8.96 | 0.15 | −2.81 | 2.83 |
| | AGB ($n = 4$) | −13.69 | 0.16 | 9.29 | 0.65 | −3.07 | 2.87 |
| | BGB ($n = 4$) | −13.37 | 0.35 | 8.01 | 1.33 | −2.54 | 4.54 |
| BMA | ($n = 4$) | −21.07 | 0.40 | 5.75 | 0.43 | 6.49 | 5.30 |

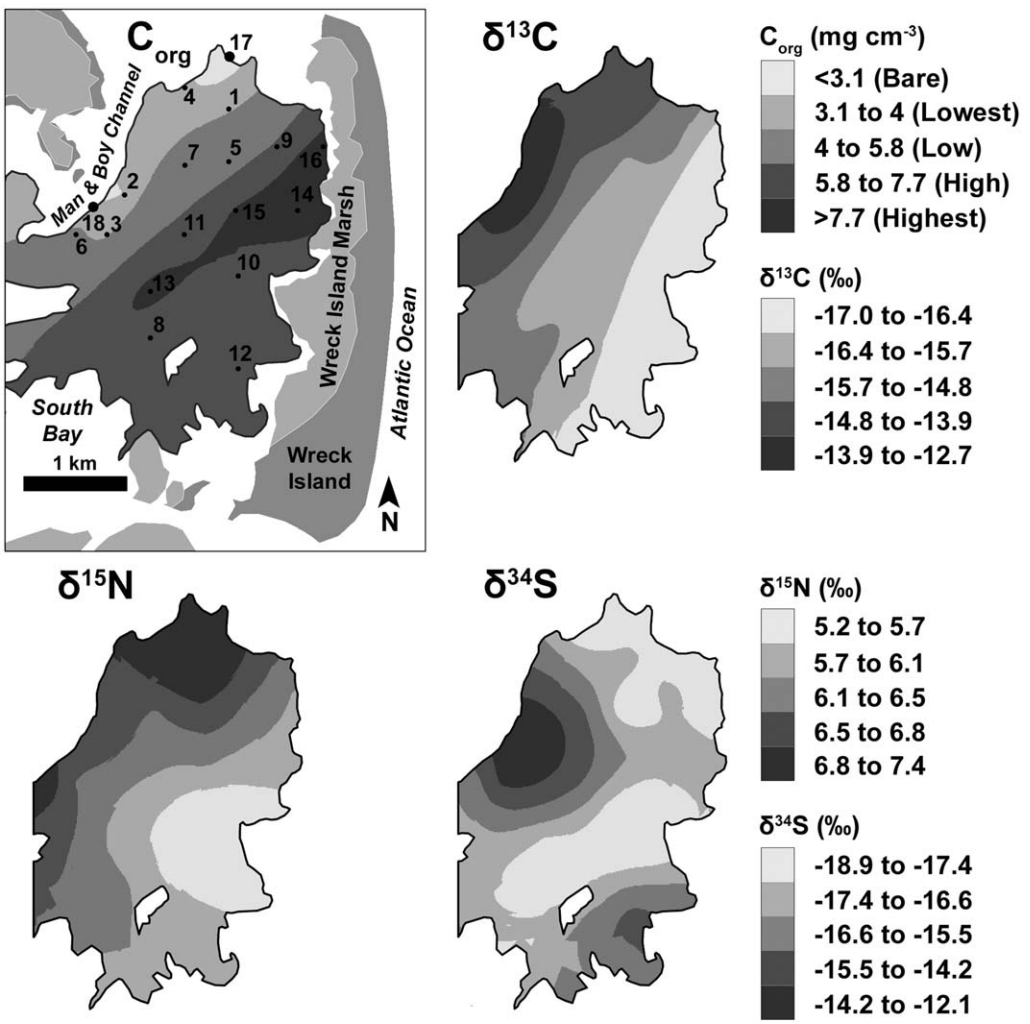


**Fig. 3.** Kriged average sediment $C_{org}$ and stable isotope ratios measured at sample sites (*see* Table 2 for site details); the $C_{org}$ distribution is shown relative to the surrounding meadow (outlined), land areas (dark gray), and marshes (light gray). Note that the sites are mapped according to the five SOC categories used in the group mixing model analysis; the group concentrations are defined in the corresponding $C_{org}$ key.

4.96‰ to 7.56‰. In comparison, the kriged $\delta^{34}S$ distribution was best fit by a spherical semivariogram but did not provide evidence for a single spatial gradient. Instead, the kriged $\delta^{34}S$ distribution suggested local enrichment zones to the northwest and to the southeast (Fig. 3). All of the $\delta^{34}S$ values showed significant depletion relative to seawater, with site values ranging from −19.12‰ to −11.86‰ (Table 2).

According to the mixing model results, different sites exhibited different autotroph source fractions (Fig. 4). Most of the individual sediment samples from the different meadow

**Table 2.** Sample site variables: Site numbers correspond to the map in Fig. 1; $C_{org}$, isotope ratio, and source fractions (posterior means) represent site averages based on three replicates; Net $C_{org}$ is the difference between the $C_{org}$ measured at meadow sites and the average bare site concentration; the distance measures relate site Euclidean distance from Wreck Island Marsh and the meadow-bare subtidal boundary (the Edge).

| Site | SOC group | $C_{org}$ (mg cm$^{-3}$) | Net $C_{org}$ (mg cm$^{-3}$) | $\delta^{13}C$ | $\delta^{15}N$ | $\delta^{34}S$ | *Zostera* fraction | *Spartina* fraction | BMA fraction | WI Marsh distance (m) | Edge distance (m) |
|---|---|---|---|---|---|---|---|---|---|---|---|
| 1 | Lowest | 3.80 | 0.95 | −13.91 | 7.56 | −17.13 | 0.369 | 0.377 | 0.254 | 800 | 345 |
| 2 | Lowest | 3.03 | 0.17 | −12.66 | 6.84 | −11.86 | 0.562 | 0.182 | 0.256 | 1703 | 134 |
| 3 | Lowest | 3.82 | 0.97 | −13.97 | 6.27 | −13.86 | 0.505 | 0.103 | 0.392 | 1699 | 284 |
| 4 | Lowest | 3.12 | 0.26 | −14.05 | 6.89 | −17.82 | 0.431 | 0.244 | 0.325 | 1171 | 25 |
| 5 | Low | 5.06 | 2.21 | −15.82 | 6.79 | −18.22 | 0.314 | 0.258 | 0.428 | 879 | 732 |
| 6 | Low | 4.28 | 1.43 | −14.56 | 7.26 | −16.39 | 0.338 | 0.343 | 0.318 | 1987 | 85 |
| 7 | Low | 5.54 | 2.69 | −15.07 | 6.27 | −15.17 | 0.447 | 0.098 | 0.455 | 1287 | 575 |
| 8 | High | 6.19 | 3.34 | −15.49 | 6.29 | −18.02 | 0.395 | 0.125 | 0.480 | 1270 | 610 |
| 9 | High | 6.01 | 3.15 | −15.59 | 6.44 | −17.07 | 0.390 | 0.127 | 0.483 | 522 | 412 |
| 10 | High | 7.23 | 4.37 | −16.45 | 4.96 | −19.12 | 0.225 | 0.272 | 0.503 | 364 | 1174 |
| 11 | High | 6.40 | 3.55 | −16.10 | 6.06 | −15.37 | 0.355 | 0.107 | 0.538 | 1009 | 803 |
| 12 | High | 6.26 | 3.40 | −16.97 | 5.83 | −14.98 | 0.245 | 0.184 | 0.571 | 451 | 362 |
| 13 | Highest | 8.37 | 5.51 | −16.21 | 5.90 | −17.57 | 0.234 | 0.289 | 0.476 | 1201 | 743 |
| 14 | Highest | 8.10 | 5.25 | −17.03 | 5.96 | −16.87 | 0.207 | 0.222 | 0.571 | 259 | 983 |
| 15 | Highest | 7.85 | 4.99 | −15.93 | 6.35 | −16.58 | 0.340 | 0.161 | 0.499 | 751 | 1121 |
| 16 | Highest | 8.51 | 5.66 | −17.02 | 6.05 | −18.60 | 0.285 | 0.095 | 0.619 | 92 | 364 |
| 17 | Bare | 2.58 | NA | −14.03 | 6.90 | −17.95 | 0.394 | 0.267 | 0.339 | 761 | −3 |
| 18 | Bare | 3.06 | NA | −13.07 | 6.63 | −14.40 | 0.529 | 0.163 | 0.309 | 1894 | −13 |

sites yielded $\delta^{13}C$ and $\delta^{15}N$ compositions intermediate between the *Z. marina*, *S. alterniflora*, and BMA end-member compositions, plotting within the $\delta^{13}C$ and $\delta^{15}N$ bi-plot mixing polygon (*see* Supporting Information for individual site bi-plots). When viewed by SOC group, sediment samples representing each group generally clustered together, but the location of the cluster within the mixing polygon shifted from closer proximity to the *Z. marina* end-member at bare and low SOC sites to the BMA end-member at higher SOC sites (Fig. 5). Samples from two "high" SOC sites (10 and 12 in Fig. 3) and two "highest" SOC sites (13 and 14) plotted outside of the mixing polygon. Omitting these four sites did not significantly alter SOC group mixing model results (Supporting Information). The remaining sites yielded well-constrained posterior distributions, but several sites (#1, 6, and 7) had posterior distribution overlap (Fig. 4).

The mixing model found good end-member posterior separation at the SOC group-level (Fig. 5; Supporting Information). The *S. alterniflora* distribution had the lowest mean value in each case; whereas, the BMA posterior mean value differed considerably among the different SOC groups (Fig. 5; Table 3). The well-constrained posterior distribution mean values allowed us to characterize the fractional contribution of each autotroph by site group. According to the mixing model, the BMA fraction increased from $0.29 \pm 0.04$ (SD) at the "lowest" SOC sites to $0.59 \pm 0.02$ (SD) at the "highest" sites. BMA contributed a fairly low fraction of the SOC at the bare control sites adjacent to the meadow, $0.32 \pm 0.07$ (SD). In comparison, the mean of the posterior distribution estimating the *Z. marina* fraction was relatively high at the bare sites, $0.51 \pm 0.10$ (SD), and decreased in the "high" and "highest" SOC groups to $0.34 \pm 0.04$ (SD) (Table 3). However, this end-member comparison did not account for the fact that total SOC also varied among the groups.

We determined *Z. marina*, *S. alterniflora*, and BMA bulk $C_{org}$ contributions for each SOC group by multiplying the group average SOC concentration by end-member fraction, represented by the posterior distribution means. *Z. marina* and BMA bulk contributions were higher at sites with higher SOC concentrations, consistent with the spatial gradient (Fig. 6). The SOC concentration attributable to *Z. marina* increased from 1.72 mg $C_{org}$ cm$^{-3}$ to 2.79 mg $C_{org}$ cm$^{-3}$, a 62% increase. The *Z. marina* bulk contribution was lowest at the bare sites (Fig. 6). The BMA SOC concentration increased even more substantially across the meadow gradient, from 1.00 mg $C_{org}$ cm$^{-3}$ to 4.84 mg $C_{org}$ cm$^{-3}$, a 384% increase. The BMA contribution at the unvegetated sites was 0.91 mg $C_{org}$ cm$^{-3}$. In comparison, the *S. alterniflora* concentration ranged from 0.26 mg $C_{org}$ cm$^{-3}$ to 1.04 mg $C_{org}$ cm$^{-3}$ but showed no consistent change across the meadow SOC spatial gradient. The estimated *S. alterniflora* concentration was approximately the same within the meadow "highest" SOC area as at the bare sites, 0.49 mg $C_{org}$ cm$^{-3}$. Despite exhibiting the highest *Z. marina* fractional contribution (Table 3),

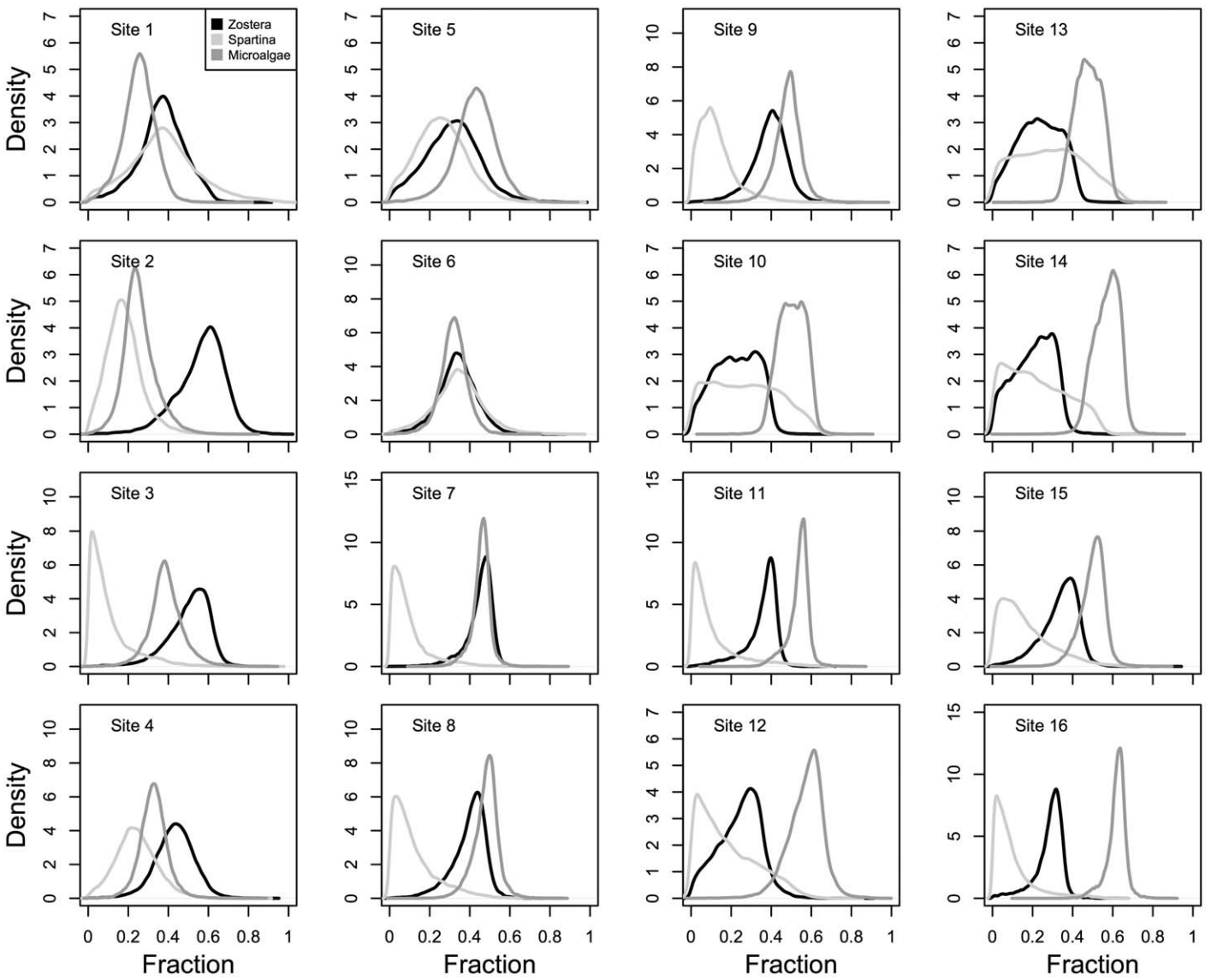


**Fig. 4.** Modeled posterior distributions for potential autotroph sources (*Z. marina*, *S. alterniflora*, and BMA) at each meadow site (*see* Fig. 1 for site locations).

the bare sites yielded the lowest *Z. marina* bulk contribution, 1.45 mg $C_{org}$ $cm^{-3}$.

By subtracting average SOC concentrations at the bare sites from the average concentrations within the "highest" area by end-member, we identified the fraction of the net SOC increase within the "highest" area attributable to each source. *Z. marina* contributed 25.3% of the net increase, *S. alterniflora* contributed $< 0.1\%$, and BMA contributed 74.5%. Averaging the end-member bulk contributions across all 16 meadow sites yielded an average *Z. marina* concentration of 2.27 mg $C_{org}$ $cm^{-3}$, an average *S. alterniflora* concentration of 0.58 mg $C_{org}$ $cm^{-3}$, and an average BMA concentration of 2.96 mg $C_{org}$ $cm^{-3}$. At the meadow-scale, *Z. marina* contributes an estimated 39.09% of the total measured stock, *S. alterniflora* contributes 9.96%, and BMA contributes 50.95%. Non-seagrass $C_{org}$, therefore, accounts for $> 60\%$ of total SOC within this bed interval, with BMA accounting for almost all ($> 83\%$) of that non-seagrass fraction.

Measured isotope ratios and autotroph source fractions (represented by the mixing model posterior means) did not show strong regression relationships with site distance from either Wreck Island Marsh or the meadow-bare subtidal edge (Table 4). The *S. alterniflora* fraction did not show a significant relationship with site distance to Wreck Island Marsh (Table 4: $p > 0.7$; Fig. 7). Relationships between the *Z. marina* and BMA fractions and distance to the meadow edge yielded $p$-values $< 0.020$. However, the *Z. marina* fraction showed an increase with proximity to this edge (Fig. 7); whereas, the BMA fraction showed an increase with distance from the edge. Omitting sites with problematic posterior distribution

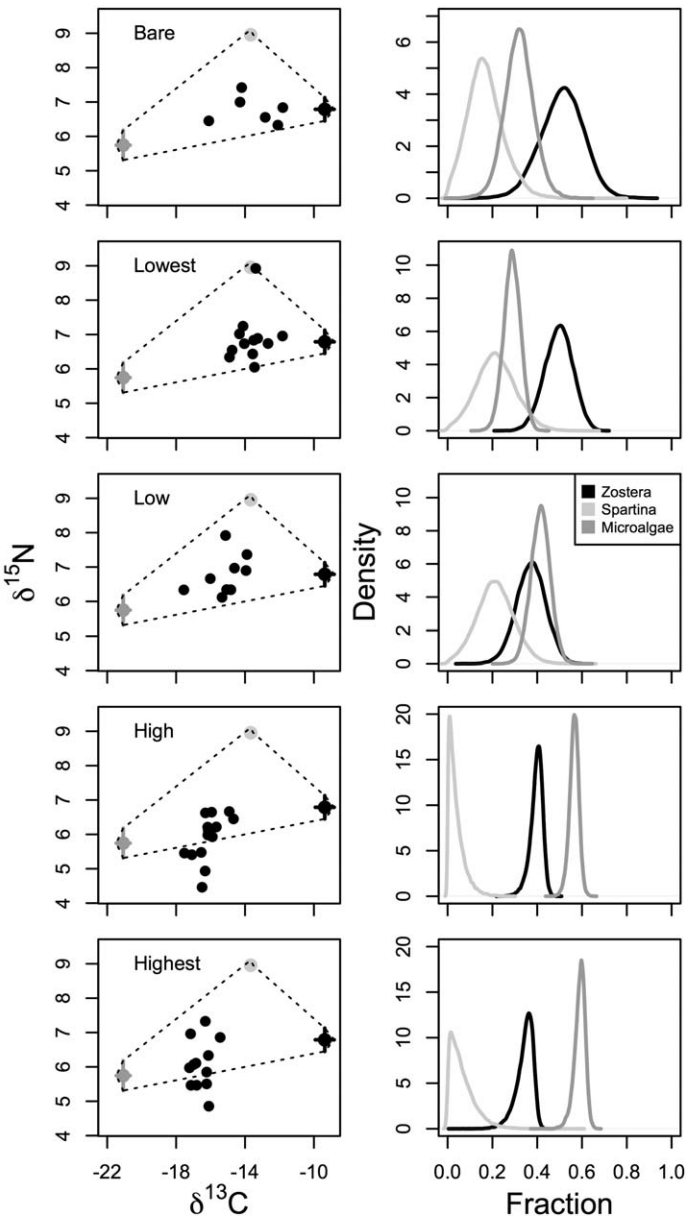


**Fig. 5.** $\delta^{13}C$ and $\delta^{15}N$ biplots, showing individual sediment samples plotted relative to the autotroph end-members ranges by SOC Group, and corresponding mixing model posterior plots.

**Table 3.** Mixing model output for each SOC group (*n*, number of sites).

| Category | *n* | $C_{org}$ (mg cm$^{-3}$) | $C_{org}$ SD | Source | Mean | SD |
|---|---|---|---|---|---|---|
| Lowest | 4 | 3.44 | 0.43 | *Zostera* | 0.50 | 0.06 |
| | | | | *Spartina* | 0.21 | 0.09 |
| | | | | BMA | 0.29 | 0.04 |
| Low | 3 | 4.96 | 0.63 | *Zostera* | 0.37 | 0.07 |
| | | | | *Spartina* | 0.21 | 0.08 |
| | | | | BMA | 0.41 | 0.08 |
| High | 5 | 6.42 | 0.48 | *Zostera* | 0.40 | 0.03 |
| | | | | *Spartina* | 0.04 | 0.04 |
| | | | | BMA | 0.56 | 0.02 |
| Highest | 4 | 8.21 | 0.29 | *Zostera* | 0.34 | 0.04 |
| | | | | *Spartina* | 0.06 | 0.06 |
| | | | | BMA | 0.59 | 0.02 |
| Bare | 2 | 2.85 | 0.25 | *Zostera* | 0.51 | 0.10 |
| | | | | *Spartina* | 0.17 | 0.08 |
| | | | | BMA | 0.32 | 0.07 |

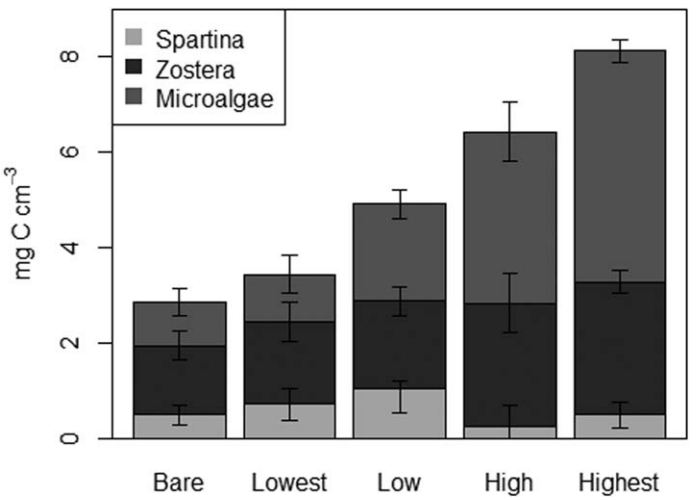


**Fig. 6.** The change in end-member bulk $C_{org}$ contributions within the restored meadow by site SOC group (*see* Fig. 3; Table 3 for information on each SOC group); error bars are the standard deviation of the source fraction posterior distribution applied to the calculation of the $C_{org}$ from each source.

results (sites 10, 12, 13, and 14) did not significantly change these regression results (Supporting Information).

## Discussion

SOC stable isotope compositions varied at different sites within this seagrass bed according to location, consistent with spatial variation in relative contributions from different carbon sources. However, the observed spatial patterns did not match the hypothesized patterns that we would expect to find if the non-seagrass SOC fraction resulted primarily from meadow burial of allochthonous POM advected into the meadow. We did not observe a *S. alterniflora* concentration gradient in the seagrass bed that decreased with distance from the nearest marsh. *S. alterniflora* POM "outwelling" did not account for the high SOC concentration in the eastern half of this meadow (hypothesis 1). Nor did we observe higher non-seagrass SOC concentrations at sites closer to bare subtidal areas, which would have supported the hypothesis that the non-seagrass fraction resulted primarily from allochthonous POM trapped by the meadow canopy (hypothesis 2). Seston trapping by the canopy may account for the *S. alterniflora* $C_{org}$ in the bed—our seston and

**Table 4.** Meadow site ($n = 16$) isotope ratio and SOC source fraction relationships with distance from Wreck Island Marsh (Marsh) and from the meadow-bare subtidal edge (Edge).

| | Intercept | SE | *M* | SE | $F_{1,14}$ | *p* | Adj-$R^2$ |
|---|---|---|---|---|---|---|---|
| $\delta^{13}$C∼Marsh | −15.450 | 0.862 | 3.27E−05 | 1.14E−03 | 0.001 | 0.978 | −0.071 |
| $\delta^{13}$C∼Edge | −15.240 | 0.621 | −3.48E−04 | 9.61E−04 | 0.131 | 0.723 | −0.062 |
| $\delta^{15}$N∼Marsh | 6.422 | 0.415 | −9.39E−05 | 5.49E−04 | 0.029 | 0.867 | −0.069 |
| $\delta^{15}$N∼Edge | 6.454 | 0.299 | −1.77E−04 | 4.63E−04 | 0.146 | 0.708 | −0.060 |
| $\delta^{34}$S∼Marsh | −17.030 | 1.263 | 7.01E−04 | 1.67E−03 | 0.176 | 0.681 | −0.058 |
| $\delta^{34}$S∼Edge | −15.603 | 0.873 | −1.71E−03 | 1.35E−03 | 1.605 | 0.226 | 0.039 |
| *Zostera*∼Marsh | 0.277 | 0.064 | 1.08E−04 | 8.52E−05 | 1.607 | 0.226 | 0.039 |
| *Zostera*∼Edge | 0.442 | 0.040 | −1.64E−04 | 6.24E−05 | 6.874 | 0.020 | 0.281 |
| *Spartina*∼Marsh | 0.182 | 0.060 | 2.47E−05 | 8.00E−05 | 0.095 | 0.763 | −0.064 |
| *Spartina*∼Edge | 0.208 | 0.044 | −1.61E−05 | 6.78E−05 | 0.056 | 0.816 | −0.067 |
| BMA∼Marsh | 0.541 | 0.070 | −1.33E−04 | 9.22E−05 | 2.073 | 0.172 | 0.067 |
| BMA∼Edge | 0.350 | 0.044 | 1.80E−04 | 6.84E−05 | 6.891 | 0.020 | 0.282 |

*S. alterniflora* biomass samples showed similar $\delta^{15}$N enrichment—but this SOC fraction was nominal (< 10%) and fairly evenly distributed both inside and outside of the meadow. Marsh POM "outwelling" was not an important source of total seagrass SOC, despite the proximity of the adjoining marsh to the seagrass bed.

The $\delta^{13}$C and $\delta^{15}$N spatial gradients we observed instead provided evidence for autochthonous, not allochthonous, $C_{org}$ burial. The *Z. marina* percent contribution was highest closer to the meadow-bare subtidal boundary and the BMA percent contribution was highest in the meadow interior. We would expect to observe the opposite pattern if the microalgal SOC fraction resulted from BMA advection into the meadow. After accounting for the bulk SOC increase across the spatial gradient, we determined that the *Z. marina* SOC concentration was actually higher in the "highest" SOC area than in the "low" and "lowest" areas (Fig. 6). The *Z. marina* percent contribution appeared to decrease with distance from the bare-subtidal edge (Fig. 7), because the BMA fraction exhibited an even larger increase at sites further from the edge (Table 4). The BMA bulk contribution was also highest at the "highest" SOC sites (Fig. 6). BMA contributed most of the $C_{org}$ to this seagrass SOC pool.

Additional sources also contribute marginally to this SOC pool, but we were ultimately unable to consider another endmember, because we were not able to include $\delta^{34}$S as a third tracer. The observed discrepancy between sediment and endmember $\delta^{34}$S ranges likely resulted from sulfate reduction within the bed, which causes similar $\delta^{34}$S depletion (Canfield 2001). Future studies may be able quantify this process and adjust measured $\delta^{34}$S values accordingly. However, we noted that the magnitude of this process varied spatially (Fig. 3), possibly due to both carbon source and bed sediment factors (cf. Oakes and Connolly 2004). We considered using the C : N ratio as a third tracer but ultimately excluded it due to possible preferential loss of N in different bed locations (Oreska et al. 2017). Absent a third tracer, we were not able to simultaneously quantify the macroalgal contribution, which Greiner et al. (2016) found to be negligible (∼ 3%), or include phytoplankton, which was likely a minor SOC contributor due to very low concentrations and productivity in the water column (McGlathery et al. 2001). Including macroalgae would not explain why samples representing four sites fell outside the biplot mixing polygon due to low $\delta^{15}$N values. The macroalgae $\delta^{15}$N range is similar to that for *S. alterniflora*, which was not a major contributor at these sites. These four sites hint at another SOC source, possibly N-fixers in the microphytobenthos or epiphyte communities (Cole and McGlathery 2012), which would explain why the site $\delta^{15}$N values were biased towards atmospheric $\delta^{15}$N. The $\delta^{15}$N ratios at these sites could also be attributable to buried phytoplankton; however, the phytoplankton collected from this system by Hondula and Pace (2014) yielded lower $\delta^{13}$C ratios (< −25‰).

Some of the BMA SOC we identified may be allochthonous, but the spatial pattern (highest contribution farthest from the meadow edge) indicates that the majority was likely fixed in situ. Hardison et al. (2013) and Timmerman (2014) documented high BMA activity within this system in bare areas, which they attributed to increased light availability at the sediment–water interface absent shading by macrophytes. Some BMA from outside the meadow might pass into the meadow in suspension before being deposited at interior meadow sites, along with other fine particulates (Hansen and Reidenbach 2012, 2013; Oreska et al. 2017). However, there is also significant BMA activity within the meadow itself. BMA produce mats of extracellular polymeric substances (EPS) that bind sediment within this meadow and help protect the bed from erosion during winter months, when seagrass shoot density is lowest (Timmerman 2014). The "high" and "highest" SOC spatial regimes correspond with areas within the meadow where diatomaceous mats are sometimes visible in aerial photographs taken by the VIMS

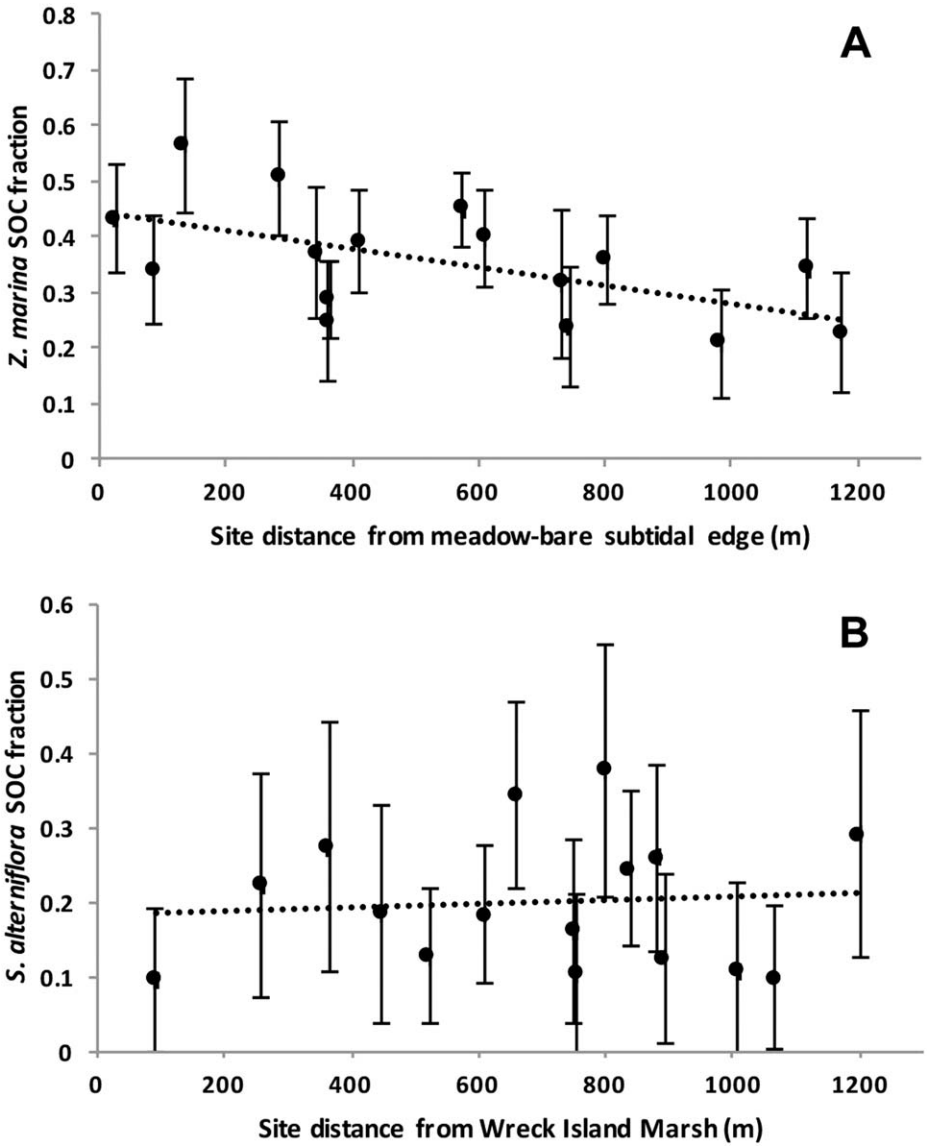


**Fig. 7.** (**A**) *Z. marina* source fraction at each site compared with site distance from the bare subtidal edge (*see* Fig. 1); (**B**) *S. alterniflora* source fraction at each site compared with site distance to Wreck Island Marsh (source fractions equal posterior means; error bars represent posterior SD; regression statistics given in Table 4).

SAV monitoring program (VIMS SAV, http://web.vims.edu/bio/sav/, accessed 12 December 2016). The 2011 photo shows this spatial correspondence distinctly, suggesting that in situ BMA production contributes to the observed SOC spatial gradient. Timmerman (2014) also measured sediment chlorophyll and carbohydrate concentrations—proxies for BMA activity—concurrent with this study at a site inside the meadow and at a bare control site. Both measures were generally higher at the meadow site. The meadow chlorophyll concentration ranged as high as 220 mg $m^{-2}$ at the seagrass site, compared with 71 mg $m^{-2}$ at the bare site; meadow carbohydrate concentrations averaged 90.2 $\mu$g $g^{-1}$ at the seagrass site, compared with 49.9 $\mu$g $g^{-1}$ at the bare site over the same period (Timmerman 2014). Consequently, most—if not all—of the BMA SOC measured in this study was likely autochthonous.

The importance of BMA as a contributor to SOC within this meadow may be due, in part, to OM recycling within the seagrass microbial community, resulting from nutrient limitation (McGlathery et al. 2004; McGlathery et al. 2007; Hardison et al. 2011). BMA turnover occurs every few days, but immediate BMA OM uptake by bacteria, and subsequent reuptake by BMA, results in tight BMA-bacterial nutrient coupling in this system, which likely facilitates OM retention in bed sediments (Hardison et al. 2013). It is, therefore, conceivable that *Z. marina* initially fixed a higher percentage of the SOC now stored within the bed, but that some of this $C_{org}$ entered the bacteria-BMA uptake cycle and now exhibits

a BMA isotopic signature. However, we do not see excessive isotope depletion consistent with multiple fractionation steps resulting from SOC recycling.

The BMA results, nevertheless, underscore the importance of considering the benthic microalgal community when constructing seagrass carbon budgets or calculating seagrass SOC burial fluxes. Studies should not assume that all—or even most—of the SOC beneath a seagrass meadow derives from seagrass. We note that BMA-derived $C_{org}$ represents a dominant SOC constituent in both vegetated and unvegetated coastal habitats (e.g., Hardison et al. 2013; Oakes and Eyre 2014), due in part to long turnover times for EPS (McKew et al. 2013; Oakes and Eyre 2014). The percentage of total seagrass production that enters the sediment carbon pool may, therefore, be significantly lower than expected based on a site's SOC profile, with the remainder of the seagrass production decomposed at the sediment surface, exported, or consumed by herbivores (Duarte and Cebrián 1996).

**Implications for blue carbon accounting**

This study is the first to document BMA contributions augmenting SOC storage in a blue carbon system. Similar studies in marsh and mangrove habitats are still lacking. Oakes and Eyre (2014) speculated that BMA may contribute significantly to the blue carbon stored in marsh, mangrove, and seagrass sediments. However, in their recent blue carbon review, Macreadie et al. (2017) only discuss microalgal carbon in the context of a regime shift from marsh or seagrass to microalgal production that results in less blue carbon storage—not coupling between these macrophytes and BMA that may increase BMA productivity and, therefore, SOC accumulation. By analyzing SOC at the meadow-scale, our results confirm initial suggestions by Greiner et al. (2016) that BMA represents the dominant contributor to the SOC stock in this particular seagrass meadow. BMA production—not allochthonous POM trapping—likely accounts for much of the non-seagrass SOC observed in seagrass meadows (Kennedy et al. 2010). We note that BMA are fairly ubiquitous in coastal habitats, even where macroalgal shading reduces light availability for photosynthesis (Hardison et al. 2011; Oakes and Eyre 2014). Seagrass canopies allow more incident light to reach the sediment surface and may, therefore, enhance BMA productivity relative to macroalgal-dominated habitats (Hardison et al. 2011, 2013).

The BMA SOC documented in this seagrass bed should be considered a carbon offset benefit of restoration provided the restored meadow either facilitates BMA presence or the burial of this material relative to bare sites. As previously noted, BMA occur at sites with and without seagrass and contribute to SOC accumulation at bare sites (e.g., Volkman et al. 2008; Hardison et al. 2013; Timmerman 2014). However, significantly higher chlorophyll and carbohydrate concentrations inside this meadow suggest BMA production is higher in the meadow than at bare control sites (Timmerman 2014). We also note that the seagrass plants facilitate bed accretion, thereby increasing the likelihood that within-meadow BMA $C_{org}$ becomes buried. According to the $^{210}Pb$ profiles, nearby bare sites are not accreting. $C_{org}$ fixed by BMA in bare areas, therefore, has a higher likelihood of being remineralized. The lower BMA SOC concentrations at the bare sites likely reflect both lower BMA production outside the meadow and lower preservation rates for that production. However, more work is needed to quantify these seagrass effects on BMA SOC burial rates.

Regarding the application of these results for seagrass offset-credit accounting (CEC 2014; Emmer et al. 2015), we note that seagrass restoration projects will not likely be able to differentiate between allochthonous and autochthonous fractions in the seagrass SOC pool with complete certainty. Our effort to differentiate these fractions in the South Bay meadow benefitted from relatively few potential end-members (Hondula and Pace 2014), low potential for diagenesis (Greiner et al. 2013), significant past work on seagrass SOC accumulation and the biotic community within the VCR-LTER system (Hardison et al. 2011, 2013; McGlathery et al. 2012) and in South Bay in particular (Greiner et al. 2013, 2016; Timmerman 2014), and a known meadow restoration history that did not include any significant bed disturbances (Orth et al. 2006, 2012; McGlathery et al. 2012). From an isotope-source modeling perspective, our results confirm that autotroph source differentiation is possible at the meadow-scale but by no means straightforward. Although we were able to constrain potential source isotope ranges and conduct a mixing model analysis, several of the posterior distributions exhibited significant spread about their means. These posterior distributions limited our ability to quantify source fractions at particular sites and, therefore, our ability to confidently quantify whole meadow stocks by source. We, consequently, refrained from kriging posterior means determined for individual sites to generate meadow-scale source maps. Some of this variability may be due to slight differences in diagenesis at individual sites or to additional sources that we were not able to include in our models. The problematic sites occur near Wreck Island (Fig. 1: sites #10, 12, 13, and 14), where macroalgae sometimes accumulates. Diagenesis is possibly a factor at sites closer to Man & Boy Channel, which yield much higher C : N ratios (Oreska et al. 2017).

Given the difficulties associated with conducting SOC source analysis, an allochthonous carbon compensation factor probably remains the best option for individual seagrass restoration projects trying to meet the CEC (2014) allochthonous carbon deduction requirement for seagrass blue carbon accounting. This study broadly supports using the Kennedy et al. (2010) 50% non-seagrass SOC compensation factor at the meadow-scale but casts doubt on whether most of that SOC is actually allochthonous. If the CEC (2014) goal is to conservatively exclude any SOC that was not fixed by the restored seagrass plants, then a 50% compensation factor applied to this meadow stock represents a reasonable deduction. However, an accurate allochthonous SOC deduction

based on this system would be closer to 10%—not 50%. Additional work may confirm that in situ BMA contribute most of the non-seagrass SOC in most seagrass meadows. Provided the storage of this production can be attributed to meadow presence, projects should be able to count this SOC as a seagrass blue carbon benefit when requesting offset-credits under the CEC (2014) accounting guidelines (Emmer et al. 2015).

## Conclusions

This study identifies spatial variability in seagrass and BMA source contributions to a seagrass SOC pool, discernable from stable isotope spatial variability evident at the seagrass meadow-scale. *Z. marina* accounts for less than half of the total SOC stock (40%); however, canopy-trapping of allochthonous POM—represented in this system primarily by *S. alterniflora*-derived seston—only accounts for another 10% of the total. Most of the SOC within this seagrass bed apparently derives from BMA that occur within the meadow. The burial and long-term storage of this SOC is at least partly attributable to seagrass presence, because the seagrass canopy facilitates bed accretion. Enhanced burial of in situ BMA $C_{org}$ should, therefore, be considered a possible blue carbon benefit of seagrass restoration. However, even with the aid of discernable stable isotope spatial gradients and isotope mixing models, quantifying the allochthonous and autochthonous SOC fractions within a seagrass bed remains somewhat speculative, because the geographic origin of SOC cannot be established with complete certainty. An allochthonous carbon compensation factor represents, perhaps, the best option for seagrass blue carbon offset-credit accounting, but the proposed 50% compensation factor would underestimate the autotrophic production fixed within this particular meadow and attributable to meadow presence. More work is needed to identify an appropriate allochthonous carbon percentage that can be generally applied to seagrass restoration projects.

## References


Appleby, P. G., and F. Oldfield. 1983. The assessment of $^{210}$Pb data from sites with varying sediment accumulation rates. Hydrobiologia **103**: 29–35. doi:10.1007/BF00028424

Bauer, J. E., W.-J. Cai, P. A. Raymond, T. S. Bianchi, C. S. Hopkinson, and P. A. G. Regnier. 2013. The changing carbon cycle of the coastal ocean. Nature **504**: 61–70. doi:10.1038/nature12857

Borges, A. V., L.-S. Schiettecatte, G. Abril, B. Delille, and F. Gazeau. 2006. Carbon dioxide in European coastal waters. Estuar. Coast. Shelf Sci. **70**: 375–387. doi:10.1016/j.ecss.2006.05.046

Bouillon, S., F. Dehairs, B. Velimirov, G. Abril, and A. Vieira Borges. 2007. Dynamics of organic and inorganic carbon across contiguous mangrove and seagrass systems (Gazi Bay, Kenya). J. Geophys. Res. **112**: G02018. doi:10.1029/2006JG000325

Bouillon, S., and R. M. Connolly. 2009. Carbon exchange among tropical coastal ecosystems, p. 45–70. *In* I. Nagelkerken [ed.], Ecological connectivity among tropical coastal ecosystems. Springer.

Cai, W.-J. 2011. Estuarine and coastal ocean carbon paradox: $CO_2$ sinks or sites of terrestrial carbon incineration? Ann. Rev. Mar. Sci. **3**: 123–145. doi:10.1146/annurev-marine-120709-142723

Campbell, J. E., E. A. Lacey, R. A. Decker, S. Crooks, and J. W. Fourqurean. 2015. Carbon storage in seagrass beds of Abu Dhabi, United Arab Emirates. Estuaries Coast. **38**: 242–251. doi:10.1007/s12237-014-9802-9

Canfield, D. E. 2001. Isotope fractionation by natural populations of sulfate-reducing bacteria. Geochim. Cosmochim. Acta **65**: 1117–1124. doi:10.1016/S0016-7037(00)00584-6

Cebrián, J., C. M. Duarte, N. Marbà, and S. Enríquez. 1997. Magnitude and fate of the production of four co-occurring Western Mediterranean seagrass species. Mar. Ecol. Prog. Ser. **155**: 29–44. doi:10.3354/meps155029

Cole, L. W., and K. J. McGlathery. 2012. Nitrogen fixation in restored eelgrass meadows. Mar. Ecol. Prog. Ser. **448**: 235–246. doi:10.3354/meps09512

Commission for Environmental Cooperation (CEC). 2014. Greenhouse gas offset methodology criteria for tidal wetland conservation. Commission for Environmental Cooperation.

Duarte, C. M., and J. Cebrián. 1996. The fate of marine autotrophic production. Limnol. Oceanogr. **41**: 1758–1766. doi:10.4319/lo.1996.41.8.1758

Duarte, C. M., H. Kennedy, N. Marbà, and I. Hendricks. 2013. Assessing the capacity of seagrass meadows for carbon burial: Current limitations and future strategies. Ocean Coast. Manag. **83**: 32–38. doi:10.1016/j.ocecoaman.2011.09.001

Emmer, I., and others. 2015. Methodology for tidal wetland and seagrass restoration. Verified Carbon Standard, VM0033 Version 1.0. [accessed 2016 June 28]. Available from http://database.v-c-s.org/methodologies/methodology-tidal-wetland-and-seagrass-restoration-v10

Flynn, W. 1968. The determination of low levels of polonium-210 in environmental materials. Anal. Chim. Acta **43**: 221–227. doi:10.1016/S0003-2670(00)89210-7

Fourqurean, J., and others. 2014. Field sampling of soil carbon pools in coastal ecosystems, p. 39–66. *In* J. Howard, S. Hoyt, K. Isensee, E. Pidgeon, and M. Telszewski [eds.], Coastal blue carbon: Methods for assessing carbon stocks and emissions factors in mangroves, tidal salt marshes, and seagrass meadows. Conservation International, Intergovernmental Oceanographic Commission of UNESCO, International Union for Conservation of Nature.

Fourqurean, J. W., and others. 2012. Seagrass ecosystems as a globally significant carbon stock. Nat. Geosci. **5**: 505–509. doi:10.1038/ngeo1477

Fry, B. 2007. Stable isotope ecology. Springer.

Gacia, E., C. M. Duarte, and J. J. Middelburg. 2002. Carbon and nutrient deposition in a Mediterranean seagrass

(*Posidonia oceanica*) meadow. Limnol. Oceanogr. **47**: 23–32. doi:10.4319/lo.2002.47.1.0023

Gattuso, J.-P., M. Frankignoulle, and R. Wollast. 1998. Carbon and carbonate metabolism in coastal aquatic ecosystems. Ann. Rev. Ecol. Syst. **29**: 405–434. doi:10.1146/annurev.ecolsys.29.1.405

Greiner, J. T., K. J. McGlathery, J. Gunnell, and B. A. McKee. 2013. Seagrass restoration enhances "blue carbon" sequestration in coastal waters. PLoS One **8**: e72469. doi:10.1371/journal.pone.0072469

Greiner, J. T., G. M. Wilkinson, K. J. McGlathery, and K. A. Emery. 2016. Sources of sediment carbon sequestered in restored seagrass meadows. Mar. Ecol. Prog. Ser. **551**: 95–105. doi:10.3354/meps11722

Hansen, J. C. R., and M. A. Reidenbach. 2012. Wave and tidally driven flows in eelgrass beds and their effect on sediment suspension. Mar. Ecol. Prog. Ser. **448**: 271–287. doi:10.3354/meps09225

Hansen, J. C. R., and M. A. Reidenbach. 2013. Seasonal growth and senescence of a *Zostera marina* seagrass meadow alters wave-dominated flow and sediment suspension within a coastal bay. Estuaries Coast. **36**: 1099–1114. doi:10.1007/s12237-013-9620-5

Harbeson, S. A. 2010. An investigation of nutrient transfer in a restored eelgrass, *Zostera marina*, meadow. Ph.D. thesis. Univ. of Virginia.

Hardison, A. K., I. C. Anderson, E. A. Canuel, C. R. Tobias, and B. Vueger. 2011. Carbon and nitrogen dynamics in shallow photic systems: Interactions between macroalgae, microalgae, and bacteria. Limnol. Oceanogr. **56**: 1489–1503. doi:10.4319/lo.2011.56.4.1489

Hardison, A. K., E. A. Canuel, I. C. Anderson, C. R. Tobias, B. Veuger, and M. N. Waters. 2013. Microphytobenthos and benthic macroalgae determine sediment organic matter composition in shallow photic sediments. Biogeosciences **10**: 5571–5588. doi:10.5194/bg-10-5571-2013

Hejnowicz, A. P., H. Kennedy, M. A. Rudd, and M. R. Huxham. 2015. Harnessing the climate mitigation, conservation and poverty alleviation potential of seagrasses: Prospects for developing blue carbon initiatives and payment for ecosystem service programmes. Front. Mar. Sci. **2**: 32. doi:10.3389/fmars.2015.00032

Heminga, M. A., F. J. Slim, J. Kazungu, G. M. Ganssen, J. Nieuwenhuize, and N. M. Kruyt. 1994. Carbon outwelling from a mangrove forest with adjacent seagrass beds and coral reefs (Gazi Bay, Kenya). Mar. Ecol. Prog. Ser. **106**: 291–301. doi:10.3354/meps106291

Hendriks, I. E., T. Sintes, T. J. Bouma, and C. M. Duarte. 2008. Experimental assessment and modeling evaluation of the effects of the seagrass *Posidonia oceanica* on flow and particle trapping. Mar. Ecol. Prog. Ser. **356**: 163–173. doi:10.3354/meps07316

Hondula, K., and M. Pace. 2011. Stable isotopes of *M. mercenaria* and plant sources on the Virginia Coast. Data publication knb-lter-vcr.200.9. [accessed 2016 July 25]. Available from https://portal.lternet.edu/nis/mapbrowse?packageid=knb-lter-vcr.200.9

Hondula, K. L. 2012. Using multiple stable isotopes including deuterium ($\delta^2$H) to trace organic matter in a complex near-shore lagoon. M.S. thesis. Univ. of Virginia.

Hondula, K. L., and M. L. Pace. 2014. Macroalgal support of cultured hard clams in a low nitrogen coastal lagoon. Mar. Ecol. Prog. Ser. **498**: 187–201. doi:10.3354/meps10644

Howard, J., S. Hoyt, K. Isensee, E. Pidgeon, and M. Telszewski. 2014. Coastal blue carbon: Methods for assessing carbon stocks and emissions factors in mangroves, tidal salt marshes, and seagrass meadows. Conservation International, Intergovernmental Oceanographic Commission of UNESCO, International Union for Conservation of Nature.

Huang, Y.-H., C.-L. Lee, C.-Y. Chung, S.-C. Hsiao, and H.-J. Lin. 2015. Carbon budgets of multispecies seagrass beds at Dongsha Island in the South China Sea. Mar. Environ. Res. **106**: 92–102. doi:10.1016/j.marenvres.2015.03.004

Hyndes, G. A., I. Nagelkerken, R. J. McLeod, R. M. Connolly, P. S. Lavery, and M. A. Vanderklift. 2014. Mechanisms and ecological role of carbon transfer within coastal seascapes. Biol. Rev. **89**: 232–254. doi:10.1111/brv.12055

Inger, R., A. Jackson, A. Parnell, and S. Bearhop. 2010. SIAR V4 (stable isotope analysis in R): An ecologists's guide. [accessed 2016 September 7]. Available from https://www.tcd.ie/Zoology/research/research/theoretical/siar/SIAR_For_Ecologists.pdf

Jankowska, E., L. N. Michel, A. Zaborska, and M. Włodarska-Kowalczuk. 2016. Sediment carbon sink in low-density temperate eelgrass meadows (Baltic Sea). J. Geophys. Res. Biogeosci. **121**: 1–17. doi:10.1001/2016JG003424

Kennedy, H., J. Beggins, C. M. Duarte, J. W. Fourqurean, M. Holmer, N. Marba, and J. J. Middelburg. 2010. Seagrass sediments as a global carbon sink: Isotopic constraints. Global Biogeochem. Cycles **24**: 1–8. doi:10.1029/2010GB003848

Macreadie, P. I., and others. 2017. Can we manage coastal ecosystems to sequester more blue carbon? Front. Ecol. Environ. **15**: 206–213. doi:10.1002/fee.1484

Matthews, K. M., C. Kim, and P. Martin. 2007. Determination of $^{210}$Po in environmental materials: A review of analytical methodology. Appl. Radiat. Isot. **65**: 267–279. doi:10.1016/j.apradiso.2006.09.005

McGlathery, K. J., I. C. Anderson, and A. C. Tyler. 2001. Magnitude and variability of benthic and pelagic metabolism in a temperate coastal lagoon. Mar. Ecol. Prog. Ser. **216**: 1–15. doi:10.3354/meps216001

McGlathery, K. J., K. Sundbäck, and I. C. Anderson. 2004. The importance of primary producers for benthic nitrogen and phosphorus cycling, p. 231–261. *In* S. L. Nielsen, G. T. Banta, and M. F. Pedersen [eds.], Estuarine nutrient cycling: The influence of primary producers. Kluwer Academic.

McGlathery, K. J., K. Sundbäck, and I. C. Anderson. 2007. Eutrophication in the shallow coastal bays and lagoons:

The role of plants in the coastal filter. Mar. Ecol. Prog. Ser. **348**: 1–18. doi:10.3354/meps07132

McGlathery, K. J., L. K. Reynolds, L. W. Cole, R. J. Orth, S. R. Marion, and A. Schwarzschild. 2012. Recovery trajectories during state change from bare sediment to eelgrass dominance. Mar. Ecol. Prog. Ser. **448**: 209–221. doi:10.3354/meps09574

McGlathery, K. J., M. A. Reidenbach, P. D'Odorico, S. Fagherazzi, M. L. Pace, and J. H. Porter. 2013. Nonlinear dynamics and alternative stable states in shallow coastal systems. Oceanography **26**: 220–231. doi:10.5670/oceanog. 2013.66

McKew, B. A., A. J. Dumbrell, J. D. Taylor, T. J. McGenity, and G. J. C. Underwood. 2013. Differences between aerobic and anaerobic degradation of microphytobenthic biofilm-derived organic matter within intertidal sediments. FEMS Microbiol. Ecol. **84**: 495–509. doi:10.1111/1574-6941.12077

Middelburg, J. J., J. Nieuwenhuize, R. K. Lubberts, and O. van de Plassche. 1997. Organic carbon isotope systematics of coastal marshes. Estuar. Coast. Shelf Sci. **45**: 681–687. doi:10.1006/ecss.1997.0247

Murray, B. C., L. Pendleton, W. A. Jenkins, and S. Sifleet. 2011. Green payments for blue carbon: Economic incentives for protecting threatened coastal habitats. Nicholas Institute for Environmental Policy Solutions Report NI R 11-04. Nicholas Institute for Environmental Policy Solutions, Duke Univ.

Nellemann, C., E. Corcoran, C. M. Duarte, L. Valdeś, C. D. Young, L. Fonseca, and G. Grimsditch. 2009. Blue carbon. A rapid response assessment. United Nations Environment Programme, GRID-Arendal.

Oakes, J. M., and R. M. Connolly. 2004. Causes of sulfur isotope variability in the seagrass, *Zostera capricorni*. J. Exp. Mar. Biol. Ecol. **302**: 153–164. doi:10.1016/j.jembe.2003. 10.011

Oakes, J. M., and B. M. A. Eyre. 2014. Transformation and fate of microphytobenthos carbon in subtropical, intertidal sediments: Potential for long-term carbon retention revealed by $^{13}$C-labeling. Biogeosciences **11**: 1927–1940. doi:10.5194/bg-11-1927-2014

Oreska, M. P. J., K. J. McGlathery, and J. H. Porter. 2017. Seagrass blue carbon accumulation at the meadow-scale. PLoS ONE **12**: e0176630. doi:10.1371/journal.pone.0176630

Orth, R. J., M. L. Luckenbach, S. R. Marion, K. A. Moore, and D. J. Wilcox. 2006. Seagrass recovery in the Delmarva Coastal Bays, USA. Aquat. Bot. **84**: 26–36. doi:10.1016/j.aquabot.2005.07.007

Orth, R. J., and K. J. McGlathery. 2012. Eelgrass recovery in the coastal bays of the Virginia Coast Reserve, USA. Mar. Ecol. Prog. Ser. **448**: 173–176. doi:10.3354/meps09596

Orth, R. J., K. A. Moore, S. R. Marion, D. J. Wilcox, and D. B. Parrish. 2012. Seed addition facilitates eelgrass recovery in a coastal bay system. Mar. Ecol. Prog. Ser. **448**: 177–195. doi:10.3354/meps09522

Regnier, P., and others. 2013. Anthropogenic perturbation of the carbon fluxes from land to ocean. Nat. Geosci. **6**: 597–607. doi:10.1038/ngeo1830

Riera, P., and P. Richard. 1996. Temporal variation of $\delta^{13}$C in particulate organic matter and oyster *Crassostrea gigas* in Marennes-Oléron Bay (France): Effect of freshwater inflow. Mar. Ecol. Prog. Ser. **147**: 105–115. doi:10.3354/meps147105

Sanchez-Cabeza, J. A., and A. C. Ruiz-Fernández. 2012. $^{210}$Pb sediment radiochronology: An integrated formulation and classification of dating models. Geochim. Cosmochim. Acta **82**: 183–200. doi:10.1016/j.gca.2010.12.024

Serrano, O., A. M. Ricart, P. S. Lavery, M. A. Mateo, A. Arias-Ortiz, P. Masque, A. Steven, and C. M. Duarte. 2015. Key biogeochemical factors affecting soil carbon storage in *Posidonia* meadows. Biogeosci. Discuss. **12**: 18913–18944. doi:10.1016/j.gca.2010.12.024

Timmerman, R. 2014. Biophysical controls on sediment suspension in a shallow coastal bay. M.S. thesis. Univ. of Virginia.

Tyler, A. C., K. J. McGlathery, and I. C. Anderson. 2001. Macroalgae mediation of dissolved organic nitrogen fluxes in a temperate coastal lagoon. Estuar. Coast. Shelf Sci. **53**: 155–168. doi:10.1006/ecss.2001.0801

Tzortziou, M., P. J. Neale, J. P. Megonigal, C. L. Pow, and M. Butterworth. 2011. Spatial gradients in dissolved carbon due to tidal marsh outwelling into a Chesapeake Bay estuary. Mar. Ecol. Prog. Ser. **426**: 41–56. doi:10.3354/meps09017

Volkman, J. K., A. T. Revill, D. G. Holdsworth, and D. Fredericks. 2008. Organic matter sources in an enclosed coastal inlet assessed using lipid biomarkers and stable isotopes. Org. Geochem. **39**: 689–710. doi:10.1016/j.orggeochem.2008.02.014

Zonneveld, K. A. F., and others. 2010. Selective preservation of organic matter in marine environments; processes and impact on the sedimentary record. Biogeosciences **7**: 483–511. doi:10.5194/bg-7-483-2010

## Acknowledgments

The authors wish to thank M. Otter at MBL and P. Luckenbach, C. Buck, A. Schwarzschild, M. Miller, A. Lunstrum, L. Aoki, and M.-L. Delgard for field and/or lab assistance. We thank J. Greiner for allowing us to reanalyze $^{210}$Pb data. R. Orth and D. Wilcox provided access to aerial imagery, and J. Porter, P. Wiberg, and R. Timmerman provided additional advice. This study was supported by National Science Foundation Virginia Coast Reserve Long Term Ecological Research Grant DEB-1237733, the University of Virginia Department of Environmental Sciences, the University of Virginia Jefferson Scholars Foundation, and by Virginia Sea Grant.

## Conflict of Interest

None declared.

*Submitted 15 March 2017*
*Revised 24 August 2017*
*Accepted 05 September 2017*

*Associate editor: Bradley Eyre*